



Effect of different environmental conditions on surface crack growth in aluminum alloys

V. Shlyannikov, R. Yarullin, I. Ishtyryakov

Kazan Scientific Center of the Russian Academy of Sciences, Russia
shlyannikov@mail.ru, yarullin_r@mail.ru, ivan_200999@mail.ru

ABSTRACT. Fatigue surface crack growth is studied through experiments and computations for aluminum alloys D16T and B95AT (analogue of 2024 and 7075 aluminum). Subjects for studies are cylindrical hollow specimens with external semi-elliptical surface crack. The variation of fatigue crack growth rate and surface crack paths behavior was studied under cyclic loading for different environmental conditions. Uniaxial tension tests were carried out at low (-60°C), room (+23°C) and high (+250°C) temperature. For the same specimen configuration and the different crack front position as a function of cyclic loading and temperatures conditions the distributions of governing parameter of the elastic-plastic stress fields in the form of I_n -factor along various crack fronts was determined from numerical calculations. This governing parameter was used as the foundation of the elastic-plastic stress intensity factor (SIF). Both elastic and plastic SIF approach was applied to the fatigue crack growth rate interpretation. It is found that there is a steady relationship between the crack growth rate and the plastic SIF in the form of general curve within a relatively narrow scatter band for all tested specimens at different temperatures.

KEYWORDS. Surface crack; Aluminum alloys; Crack growth; Environmental conditions; Fatigue fracture diagram; Plastic SIF.



Citation: Shlyannikov, V., Yarullin, R., Ishtyryakov, I., Effect of different environmental conditions on surface crack growth in aluminum alloys, 41 (2017) 31-39.

Received: 28.02.2017

Accepted: 15.04.2017

Published: 01.07.2017

Copyright: © 2017 This is an open access article under the terms of the CC-BY 4.0, which permits unrestricted use, distribution, and reproduction in any medium, provided the original author and source are credited.

INTRODUCTION

The circular cylindrical metallic components of aircraft structure, power engineering elements, pressure vessel and piping are subjected to temperature variations from -60°C (213K) to more than 250°C (523K). In most cases, part-through flaws appear on the free surface of the cylinder and defects are approximately considered as semi-elliptical cracks. The fatigue growth analysis of surface cracks under different environmental conditions is very important for many engineering applications in order to quantify the structural safety according to the so-called damage tolerant design. Furthermore, other environmental effects should be taken into account to assess the structural component safety: for example, the humidity and salt air content play an important role especially under fatigue loading.



In this paper, only the temperature effects are considered and the fatigue crack propagation is examined. Firstly, main mechanical properties of considered alloys are determined on different temperature conditions. Secondly, experimental results of fatigue crack growth for a crack starting from a semi-elliptical edge notch in cylindrical hollow specimens under low/high and room temperature are given. The relations of crack mouth opening displacement (CMOD) and crack length on the free surface of specimens are obtained. Using the aforementioned relations, the crack front shape and crack growth rate in the depth direction can be predicted. Third, constrain parameters behaviour and governing parameter of elastic-plastic stress field distribution along the crack front was obtained using FEM analysis. Crack growth interpretation is performed using the traditional elastic and new plastic SIF [1-3]. It is found that there is a steady relationship between the crack growth rate and the plastic SIF in the form of general curve within a relatively narrow scatter band for all tested specimens at different temperatures.

SPECIMENS AND MATERIAL PROPERTIES

The crack growth rate tests were carried out for cylindrical hollow specimens with semi-elliptical surface cracks. The hollow cylindrical specimen geometry configuration is shown in Fig. 1a. The diameter is equal to 28 mm in the test section and the length is equal to 130 mm. Using electro spark method surface edge cracks were cut with initial flaw depths equal to 3.0mm. The geometric parameters of the specimen test section and of the growing crack are shown in Figs. 1b. In this figure, b is the current crack depth, with the crack front approximated by an elliptical curve with major axis $2c$ and minor axis $2a$. The crack length b is obtained by measuring the distance between the advancing crack break through point and the notch break through point. The depth of the initial curvilinear edge notch is denoted by a and the initial notch length by h . Both the optical microscope measurements and the crack mouth opening displacement (CMOD) method are used to monitor and calculate both crack depth and crack length during the tests. The CMOD is measured on the free hollow specimen cylindrical surface, in the central plane of symmetry as shown in Fig. 1c.

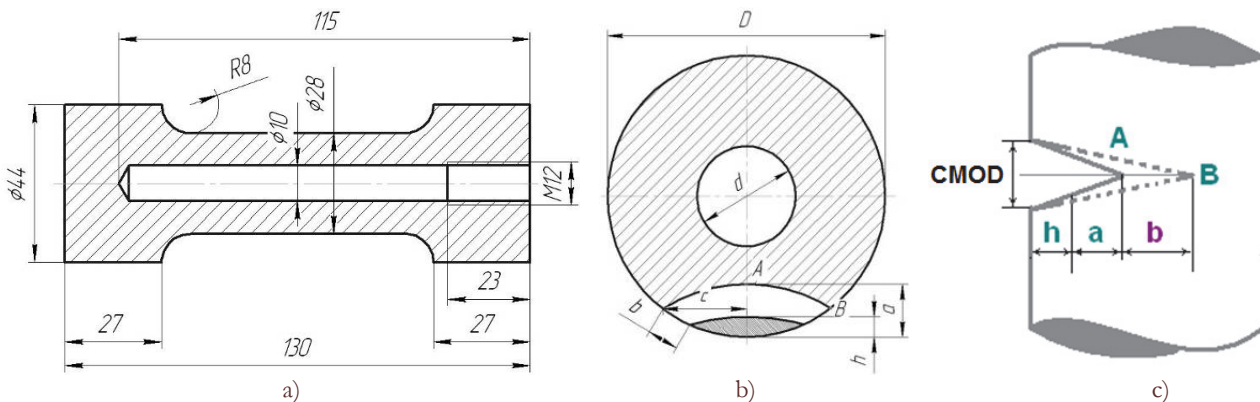


Figure 1: Details of the hollow specimen geometry and initial notch.

The test materials are most popular in aircraft industry aluminum alloys D16T and B95AT (analogue of 2024 and 7075 aluminum). All tests were carried out at room (23°C or 296K), low (-60°C or 213K) and high (250°C or 523K) temperature with sinusoidal loading form with load control. Low/high temperature tests were performed by using following equipment: *Bi-00-101 UTM Test System* with fatigue rated axial dynamic load cell (capacity +/- 50kN) and *Bi-06-303* series axial extensometer; Climatic Chamber *CM Envirosystems* with temperature range: -60°C to 250°C (Fig.2). For the cyclic tension fatigue tests, the specimens are tested with an applied maximum nominal stress equal to 65 MPa and with a frequency value 10 Hz.

The main mechanical properties of considered alloys were determined in accordance with ASTM E8 for each temperature level [4]. Obtained main mechanical properties are listed in Tab. 1, where E is the Young's modulus, σ_s is the nominal ultimate tensile strength, σ_0 is the monotonic yield strength, σ_u is the true ultimate tensile strength, δ is the elongation, ϕ is the reduction of area, n is the strain hardening exponent and α is the strain hardening coefficient.



Figure 2: Low/high temperature test equipment.

Material	Temperature, °C	σ_0 , MPa	σ_s , MPa	σ_u , MPa	α	n	E, GPa	δ , %	ψ , %
D16T	-60	406	545	633	2.56	5.32	79.232	15	17
	+23	438	594	665	1.54	5.86	76.557	11	11
	+250	294	339	371	1.44	8.39	75.246	4	27
B95AT	-60	506	621	694	1.64	7.71	75.935	11	13
	+23	520	586	775	1.44	10.37	75.274	14	36
	+250	415	422	436	1.22	12.00	72.737	6	37

Table 1: Main mechanical properties of aluminum alloys under different temperature.

Features of the tests in climatic chamber

The fatigue surface crack growth rate study for different environmental conditions has several limitations. Firstly, measurements of crack length b on free surface of specimens by microscope for the test in climatic chamber sometimes are impossible. Secondly, determination of crack size by compliance is not correct, because for surface flaws the crack growth rate value changes along the crack front from the free surface toward the mid-plane.

Therefore, two different stress ratio R values (0.1 and 0.5) are applied several times to the specimens in order to fix current crack front position: during each test, beach marks are produced on each specimen by increasing the applied stress ratio from 0.1 to 0.5 at a constant value of the maximum cyclic nominal stress, when the surface crack length is approximately increased to $b \approx 0.1$ mm. In this manner the marker loading does not induce load history effects or overload retardation [5, 6]. The typical surface marks on the fracture cross section of specimens are shown in Fig. 3 for different temperature conditions.

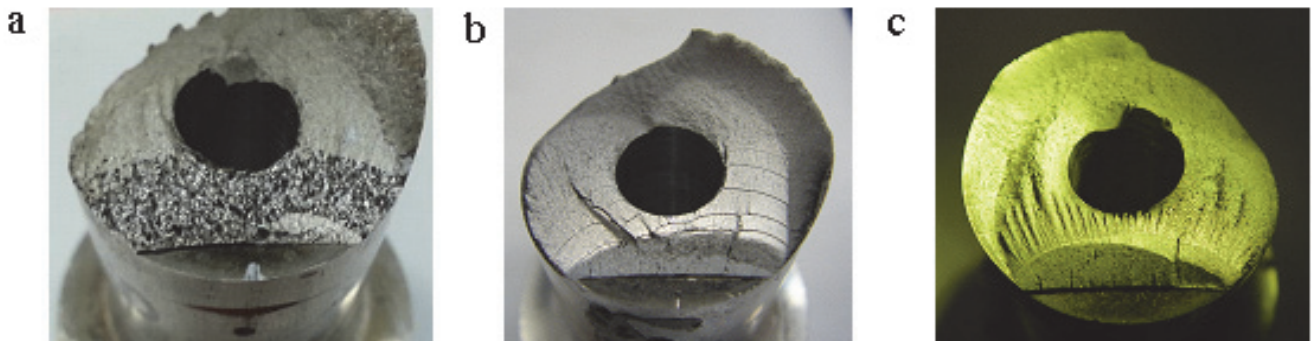


Figure 3: Fracture surface of the hollow specimens at different temperatures: (a) -60°C, (b) +23°C, (c) +250°C.



From the crack front shape obtained in this way, the relations between the relative crack depth a/D and the surface crack chord length b/D can be measured using a comparison microscope (Fig. 4). In addition, based on periodically measured increments of surface crack chord length Δb , the curve of surface crack propagation versus cycle numbers db/dN can be obtained. Afterwards, utilizing the relation of crack depth versus surface crack chord length, it is possible to obtain the crack growth rates da/dN in the depth direction.

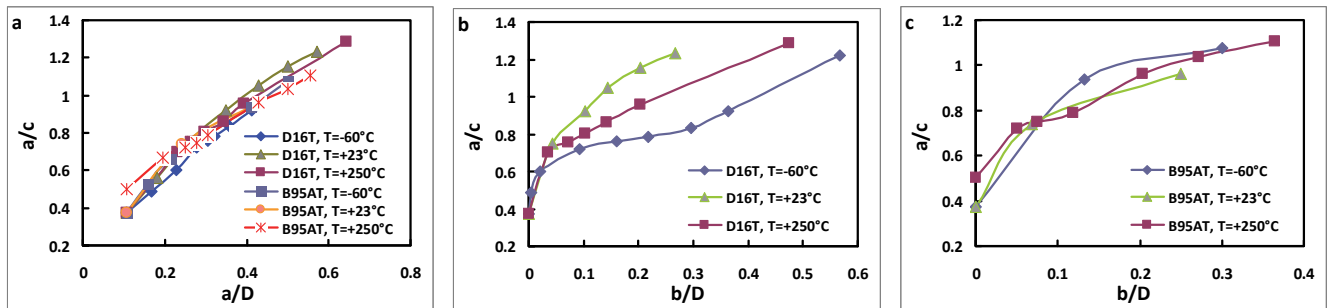


Figure 4: Aspect ratio versus crack depth (a) and crack length (b, c) for both alloys and different temperature conditions.

The evolution of the crack growth rate of the elliptical-fronted edge cracks during the tests is determined using CMOD and the microscope. Fig. 5 shows relations between CMOD and crack length b on free surface for both alloys and three temperatures. It is found strong correlation between these two parameters which can be very useful for automation of experimental studies of fatigue and fracture under multiaxial stress state. It should be noted, that the measurements of crack length b by microscope on free surface of specimens for the test in climatic chamber are impossible. For these specimens crack length b was obtained on the base of experimental relations represented on Fig. 5.

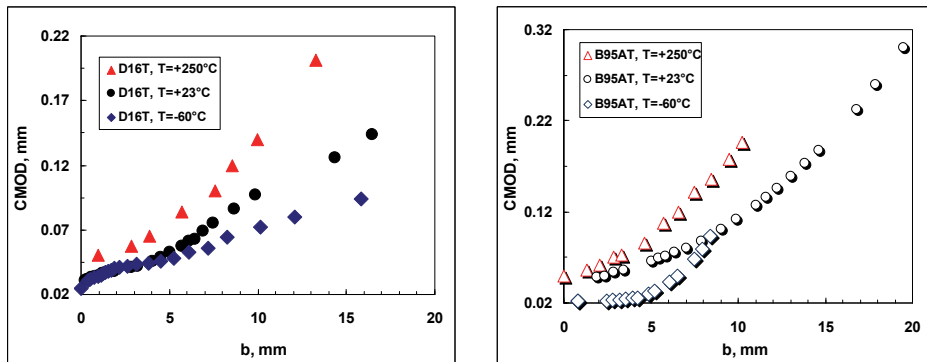


Figure 5: Relationship between CMOD and crack length on free surface of hollow specimen under different temperature conditions.

NUMERICAL STUDY

The main purpose of the present study is the interpretation of the surface crack growth rate data in terms of elastic and plastic fracture mechanics parameters. In our previous work we calculated different constraint parameters distribution along the crack front. That is the elastic constraint parameters in the form of the non-singular T -stress and T_Z -factor as well as the elastic-plastic constraint parameters in the form of local stress triaxiality b and I_n -factor for the specified combinations of tested material and temperature conditions [4].

FEM analysis was performed for semi-elliptical cracks in the cylindrical hollow specimens to determine the stress strain fields along the crack front. Typical finite element meshes for the cylindrical hollow specimens are illustrated in Fig. 6. The stress-strain state and constraint parameters at the crack tip for each type of the tested specimens were calculated by using the corresponding static material properties listed in Tab. 1, ranges of the testing loads and temperatures. These distributions correspond to the crack front positions at the accumulated number of loading cycles: initial front, intermediate front and final failure front (Fig. 7). One of the purposes of the work is to obtain an accurate description for the distribution along the crack front of the governing parameter of the elastic-plastic solution in the form of an I_n -integral

and to determine the accuracy of this type of calculation, which will be used later for the general 3D problem to provide for the plastic SIF.

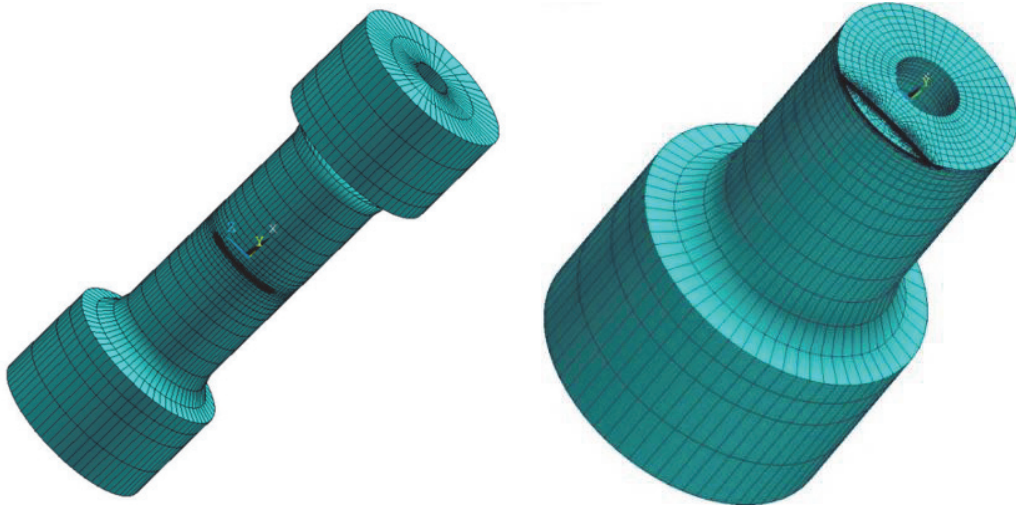


Figure 6: Typical FEM-mesh for cylindrical hollow specimens with semi-elliptical surface crack.

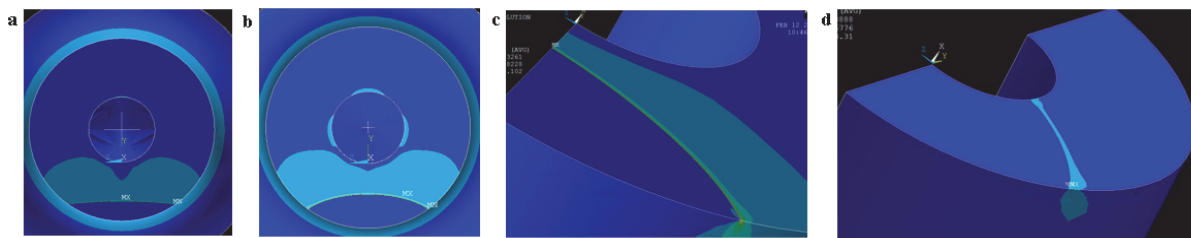


Figure 7: FEM crack front geometry: initial (a), intermediate (b, c), final (d).

The distributions of I_n -integral along the crack front were used to determine the plastic SIF K_p . For cylindrical hollow specimens the plastic SIF K_p in pure Mode I can be expressed directly in terms of the corresponding elastic SIF K_1 using Rice's J-integral as follows:

$$J = \frac{\left(K_1^2\right)}{E'} = \frac{\bar{\alpha}\sigma_0^2}{E'} I_n(\theta)(K_P)^{n+1} \quad (1)$$

$$\bar{K}_p = \left[\frac{K_1^2}{\bar{\alpha}\sigma_0 I_n^{FEM}(\theta, n, (a/w))} \right]^{1/(n+1)} = \left[\left(\frac{\sigma}{\sigma_0} \right)^2 \frac{\pi(a/w)}{\bar{\alpha}} \frac{Y_1^2(a/w)}{I_n^{FEM}(\theta, n, (a/w))} \right]^{1/(n+1)} ; \bar{K}_1 = \sigma \sqrt{\pi \lambda} \cdot Y_1(a/w) \quad (2)$$

where $\bar{K}_1 = K_1 / \sqrt{w}$ is normalized by a characteristic size of cracked body elastic stress intensity factor and $E' = E$ for plane stress and $E' = E / (1 - \nu^2)$ for plane strain. In the above equations, $\bar{\alpha}$ and n are the hardening parameters, $\lambda = a/w$ is the dimensionless crack length, w is characteristic size of specimen (for our case that is specimen diameter), σ is the nominal stress, and σ_0 is the yield stress. The procedure for calculating of the governing parameter of the elastic-plastic stress-strain fields in the form of I_n -integral for the different specimen geometries by means of the elastic-plastic FE-analysis of the near crack-tip stress-strain fields suggested by [1-3]. In this case, the numerical integral of the crack tip field I_n changes not only with the strain hardening exponent n but also with the relative crack length b/D and the relative crack depth a/D :



$$I_n^{\text{FEM}}\left(\theta, n, \left(\frac{b}{D}, \frac{a}{D}\right)\right) = \int_{-\pi}^{\pi} \left\{ \frac{n}{n+1} \left(\tilde{\sigma}_e^{n+1} \right)^{\text{FEM}} \cos \theta - \left[\tilde{\sigma}_{rr}^{\text{FEM}} \left(\tilde{u}_\theta^{\text{FEM}} - \frac{d\tilde{u}_r^{\text{FEM}}}{d\theta} \right) - \tilde{\sigma}_{r\theta}^{\text{FEM}} \left(\tilde{u}_r^{\text{FEM}} + \frac{d\tilde{u}_\theta^{\text{FEM}}}{d\theta} \right) \right] \sin \theta - \right. \\ \left. - \frac{1}{n+1} \left(\tilde{\sigma}_{rr}^{\text{FEM}} \tilde{u}_r^{\text{FEM}} + \tilde{\sigma}_{r\theta}^{\text{FEM}} \tilde{u}_\theta^{\text{FEM}} \right) \cos \theta \right\} d\theta \quad (3)$$

where $\tilde{\sigma}_{ij}$ - dimensionless stress components, \tilde{u}_i - dimensionless displacement components, r, θ - polar coordinates.

The distributions of the elastic and plastic SIF along the initial crack front for both alloys and three temperatures are plotted in Fig. 8. The constraint parameters are plotted against the normalized coordinate RR. In this plot $RR = 0.0$ is the specimen free surface, $RR = 1.0$ is the mid-plane of the hollow specimen thickness. It can be observed, that all constraint parameters essentially changed along the crack front from the free surface toward to mid-plane.

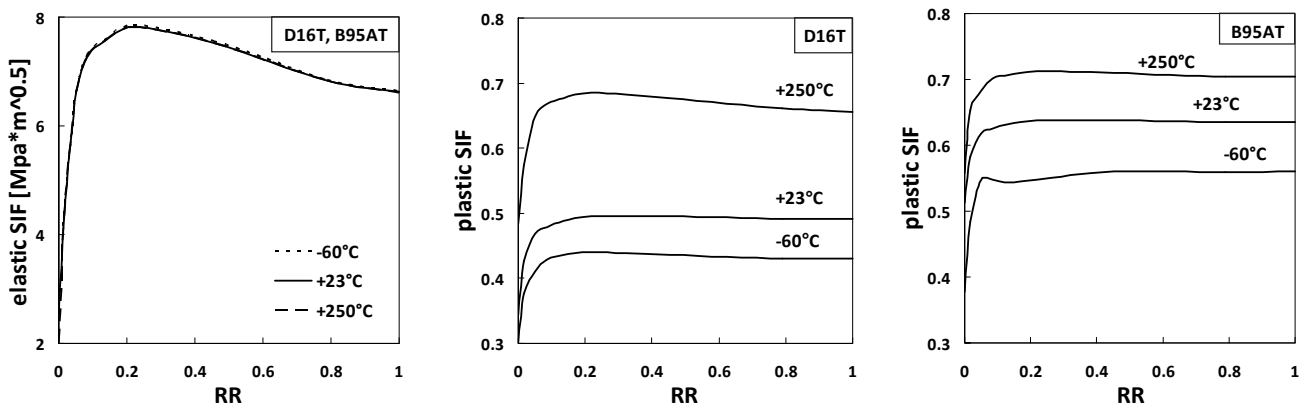


Figure 8: Elastic and plastic SIF distributions for initial crack front.

Fig. 8 gives a clear illustration of the necessity to take into account the plastic properties of the material in the interpretation of the characteristics of the material resistance to crack propagation. The distributions of elastic SIF are the same for both tested materials, because elastic properties of tested materials approximately the same (Tab. 1). Contrary to that, the plastic SIF shows very useful effect of the sensitivity to the plastic properties of the tested materials. It can be seen from Fig. 8 that the plastic SIF gradually increases by increasing the test temperature conditions. The data presented very obvious advantages of using the plastic SIF to characterize the material's resistance to cyclic crack growth. Numerical data for the elastic and plastic SIF behaviors accounting for the material properties and temperature conditions will be used to interpret the characteristics of the material resistance to crack propagation.

EXPERIMENTAL RESULTS AND DISCUSSION

The first part of experimental results includes the data of direct measurements of the objective parameters such as the crack length b and the CMOD on the free surface of specimens for all considered alloys and temperature conditions. Fig. 9 represents the surface crack growth rate db/dN versus CMOD on the hollow cylindrical specimens. It is found that the crack growth rate along the external surface direction as a function of CMOD described by a various curves with a small scatter band of the experimental results for both tested aluminum alloys. Also, looking at Fig. 4b, 4c and considering changes in the general durability of the specimens in low/high temperature test, significant differences in the crack growth rate in the depth direction a and on the free surface b of hollow specimens under the above temperature conditions are expected.

The second part of the experimental data relates to the interpretation of the surface crack growth rate for aluminum alloys at different temperature conditions with the involvement of the numerical results for elastic and plastic SIF's distributions presented in the previous section of this paper.

Based on the interpretation of experimental fatigue fracture diagrams in terms of traditional elastic SIF it is found that there are three separate diagrams for each temperature on the free surface of the hollow cylindrical specimen (Fig. 10a). In

contrast, by interpretation of the same experimental crack growth rate diagrams in terms of plastic SIF for free surface of the hollow cylindrical specimens of D16T at $-60^{\circ}\text{C} \div +250^{\circ}\text{C}$ temperatures a different picture is observed. It is shown that the individual test results at a fixed temperature form a common experimental curve partially overlapping crack growth rate ranges.

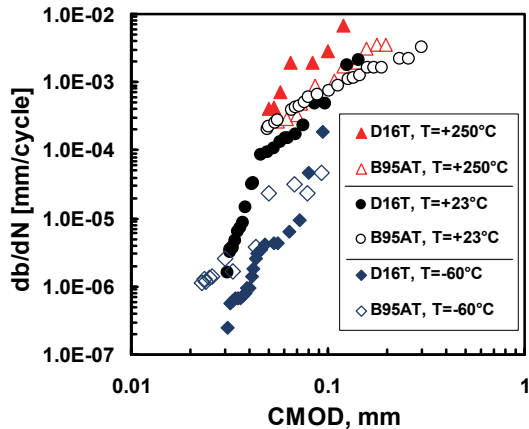


Figure 9: Crack growth rate on the free surface of hollow specimen versus CMOD for different temperature conditions.

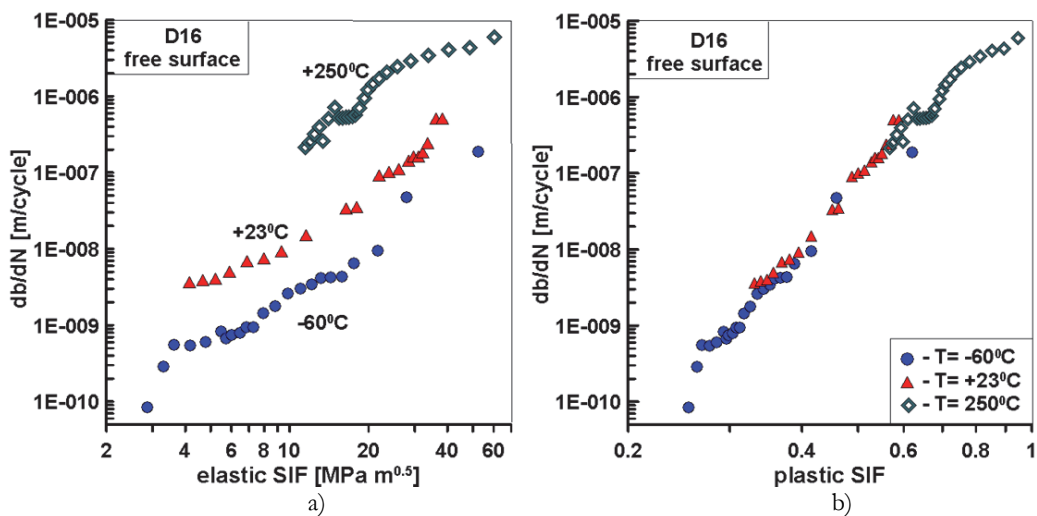


Figure 10: Crack growth rate as a function of (a) elastic and (b) plastic SIFs for free surface of the specimen.

The same trend observed for the deepest point of the crack front (Fig. 11a, b).

Moreover, compared with an elastic interpretation of the processes of fatigue failure, the interpretation of cyclic fracture diagrams in terms of the plastic SIF's has more uniform character with a small scatter band. The data presented very obvious advantages of using the plastic SIF's to characterize the material's resistance to cyclic crack growth. This conclusion is confirmed by the relative position of crack growth curves in Figs.10 and 11 for the tested aluminum alloy D16T in the terms of the elastic and the dimensionless plastic SIF K_p .

Fig. 12 shows the influence of material properties. On this figure the comparison of crack growth data on the free surface in terms of elastic and plastic SIF for both tested materials are presented. Experimental data interpretations in terms of plastic SIF, which take into account the influence of plastic material properties, give us two different curves for considered alloys.

From Fig. 12b, the difference in the crack growth rate on the D16T and B95AT remains permanently during low temperature and gradually disappears during room temperature test condition. As presented in Fig. 12, the experimental data clearly illustrates the effect of temperature on the surface crack growth rate in aluminum alloys tested at the same loading conditions.

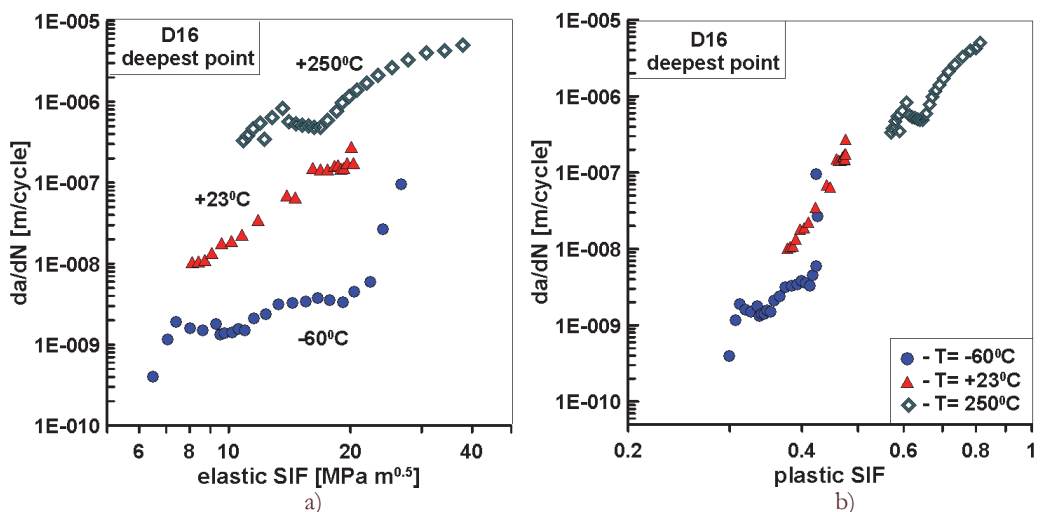


Figure 11: Crack growth rate as a function of (a) elastic and (b) plastic SIFs for deepest point of the crack front.

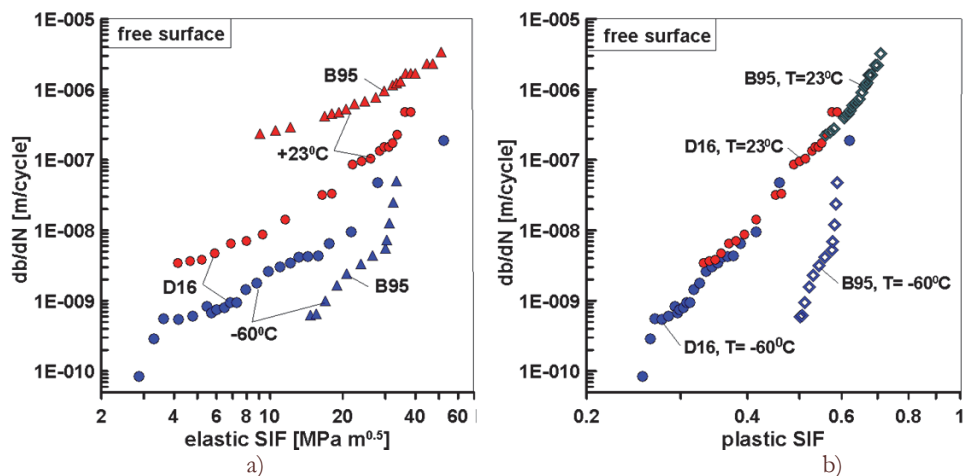


Figure 12: Crack growth rate as a function of (a) elastic and (b) plastic SIFs for both alloys and different temperature conditions.

CONCLUSIONS

Fatigue surface crack growth is studied through experiments and computations for aluminum alloys D16T and B95AT (analogue of 2024 and 7075 aluminum). For both alloys the increasing of test temperature leads to degradation of mechanical properties. By experimental studies for considered temperature conditions the relations between the crack sizes on the free surface of specimen, CMOD, crack growth rate and aspect ratio were obtained. For the same specimen configuration and the different crack front position the elastic and elastic-plastic constraint parameters were analyzed as a function of material properties and temperatures conditions. It is stated that the plastic SIF, which is sensitive to the constraint effects and elastic-plastic material properties, is attractive as the self-dependent unified parameter for characterization of the material fracture resistance properties.

REFERENCES

- [1] Shlyannikov, V.N., Tumanov, A.V., Characterization of crack tip stress fields in test specimens using mode mixity parameters, *Int. J. Fract.*, 185 (2014) 49-76.
- [2] Shlyannikov, V.N., Zakharov, A.P., Multiaxial crack growth rate under variable T-stress, *Eng. Fract. Mech.*, 123 (2014) 86-99.



- [3] Shlyannikov, V.N., Tumanov, A.V., Zakharov, A.P., The mixed mode crack growth rate in cruciform specimens subject to biaxial loading, *Theoret. Appl. Fract. Mech.*, 73 (2014) 68-81.
- [4] Yarullin R., Ishtyryakov I., Fatigue surface crack growth in aluminum alloys under different temperatures, *Procedia Engineering*, Vol. 160, 2016, 199–206.
- [5] Slyannikov, V., Yarullin, R., Ishtyryakov, I., Surface crack growth in cylindrical hollow specimen subject to tension and torsion, *Frattura ed Integrità Strutturale*, 33 (2015) 335-344.
- [6] Shlyannikov, V., Tumanov, A., Zakharov, A., Gerasimenko, A., Surface flaws behavior under tension, bending and biaxial cyclic loading, *Int. J. Fatigue*, 92 (2) (2016) 557-576.